Chapter 6

Molecular Salts of Antibiotic Drug Trimethoprim to Modify its Solubility and Membrane Permeability

6.1 Abstract

The synthesis of six molecular salts of the antibiotic drug trimethoprim (TRM) with improved solubility and membrane permeability is demonstrated in this chapter. The drug suffers from low bioavailability as it is under the category of BCS class II. Multicomponent crystals of the drug were synthesized with isomeric monohydroxybenzoic acids (HBA) and monoaminobenzoic acids (ABA) through liquid-assisted grinding with ethanol. The product materials were analyzed using various analytical techniques. The solid-state formulations improved the solubility and membrane permeability of the drug. The variation in the strength of the structure forming interactions as well as the stability of molecular packing have a significant impact on the properties of the molecular salts. Apart from that, the lipophilicity change manifested by the percentage contribution of noncovalent interactions and conformation change in the parent API are key factors that attributed to the improvement of the desired properties.

6.2 Introduction

Solubility has a key role in drug efficiency since it determines the bioavailability of pharmaceuticals together with the membrane permeability [1,2]. The formulation of a drug with optimal solubility and permeability parameters is vital for its effective delivery and efficacy. These properties mainly depend on the noncovalent interactions that control the crystal packing in the solid-state and lipophilic nature of the drug. Lipophilicity facilitates the permeation of oral drugs via cell membrane by offering ample interaction with media and membrane [3–5]. On the other hand, lipophilic drugs display poor aqueous solubility that results in low oral bioavailability. Modification of intermolecular interactions via crystal engineering has become an effective method used for changing the molecular packing in the solid state and lipophilicity to modulate the physicochemical properties of drugs [6–16]. The nature of the coformer and its interaction with the drug molecule determine the properties of the multicomponent crystals. Therefore, the selection of appropriate coformers during the design and synthesis of the multicomponent crystals is vital to obtain the desired properties. Generally, highly soluble coformers yield multicomponent products with high solubility, whereas incorporating highly lipophilic

coformers in the crystal lattice of the drug increases its permeation behavior [17,18]. The physicochemical property can be also modulated by adjusting the drug conformation via cocrystallization [19,20]. The role of drug conformation change on the solubility and membrane permeation of molecular salts of conformationally flexible famotidine and isomeric coformers has been demonstrated in Chapter 3. This chapter covers a study on the physicochemical properties of molecular salts of trimethoprim (TRM) with benzoic acid derivatives as coformers (Scheme 6.1). TRM is an essential antibiotic drug commonly used in the medication of bladder infections. The availability of the drug in the body is limited due to its low solubility (BCS class II drug), as a result, higher dosages of the drug are prescribed. CSD survey reveals that 73 salts and cocrystals of trimethoprim have been reported of which only a few of them are studies on property improvement (see Table 5.1 in Chapter 5). Salt of TRM and malic acid demonstrated improved solubility and antibacterial activity in comparison to the pure API [21]. The solubility of TRM was improved through the salt formation with fenamic acids and nicotinamide as coformers [22,23]. Cocrystal of trimethoprim with nitrofurantoin demonstrated better solubility and antimicrobial activity than that of the two starting materials [24]. Dimorphic salts involving trimethoprim and D-/L-lactic acid as coformer displayed a 5-fold increment in solubility [25]. The molecular salts of TRM presented in this chapter show improved solubility and membrane permeation at pH 1.2 and 7.4. Isomeric hydroxybenzoic acids (HBA) and aminobenzoic acids (ABA) are considered as coformers to synthesize the molecular salts of TRM. The formation of different hydrogen bonding interactions between drug and coformers, the change in the lipophilic nature, and the conformational change in the drug play a key role in regulating the solubility and permeability parameters.

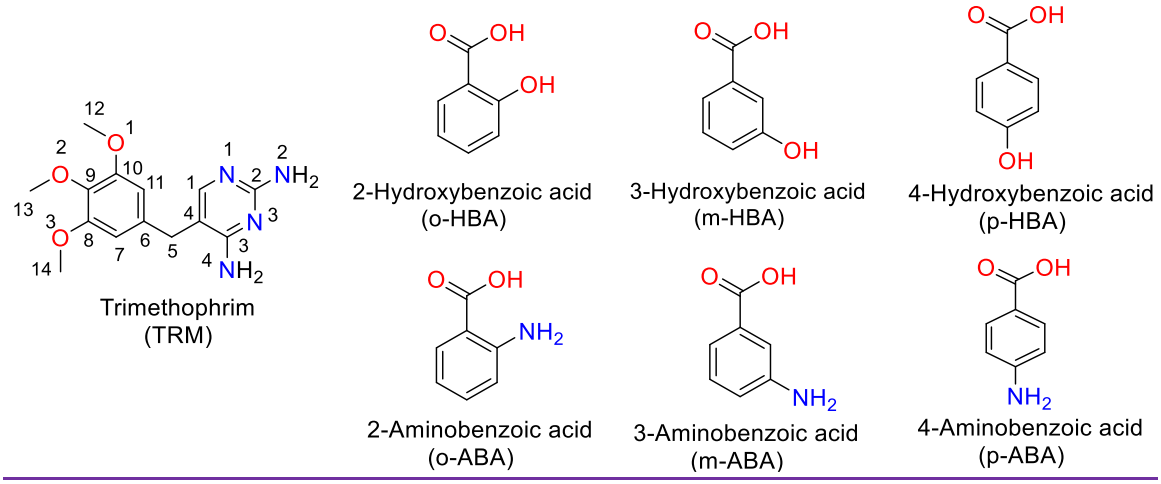

Scheme 6.1 Molecular structures of the drug trimethoprim and coformers.

6.3 Results and Discussion

6.3.1 Synthesis of Molecular Salts

Trimethoprim (pK_a = 7.12) usually forms a two-point hydrogen bonding with acids through aminopyrimidine and carboxylic acid groups [26–28]. Using crystal engineering principles, six molecular salts of TRM were synthesized and characterized using FTIR, DSC, TGA, PXRD, and single crystal X-RD. The products were obtained in a 1:1 ratio of the drug and coformers with different water molecules of crystallization ratios in their structures (Table 6.1). Only the structure of TRM-4 was isolated in anhydrous form. The objective of the study is to understand the role of OH and NH_2 and their isomeric positions in tailoring the physicochemical properties of salts of trimethoprim.

Table 6.1. The multicomponent solids of drug TRM with isomeric HBA and ABA and their stoichiometric ratio.

API	coformer	product	stoichiometric ratio	crystallization solvent
TRM	2-Hydroxybenzoic acid	TRM-1	1:1:3 [TRM:*o*-HBA:H_2O]	2MeOH : 3ACN
	3-Hydroxybenzoic acid	TRM-2	1:1:1 [TRM:*m*-HBA:H_2O]	MeOH
	4-Hydroxybenzoic acid	TRM-3	1:1:2 [TRM:*p*-HBA:H_2O]	ACN
	2-Aminobenzoic acid	TRM-4	1:1 [TRM:*o*-ABA]	MeOH
	3-Aminobenzoic acid	TRM-5	1:1:2 [TRM:*m*-ABA:H_2O]	-
	4-Aminobenzoic acid	TRM-6	1:1:2 [TRM:*p*-ABA:H_2O]	MeOH

6.3.2 Characterization of Product Phases

Vibrational Spectroscopy (FT-IR). The comparison of IR spectra of product materials TRM-1 to TRM-6 with that of the pure TRM is plotted in Figure 6.1. The stretching frequencies of major functional groups for the drug and its multicomponent crystals are listed in the experimental section 6.5.3. A significant shift in the N–H absorption bands shows the formation of extended hydrogen bond interactions between TRM and coformers. The appearance of new strong IR absorption peaks near 1400 cm^{-1} indicates the formation of a carboxylate anion because of a proton transfer from the COOH group of coformers to one of the basic N atoms of the pyrimidine ring in the TRM.

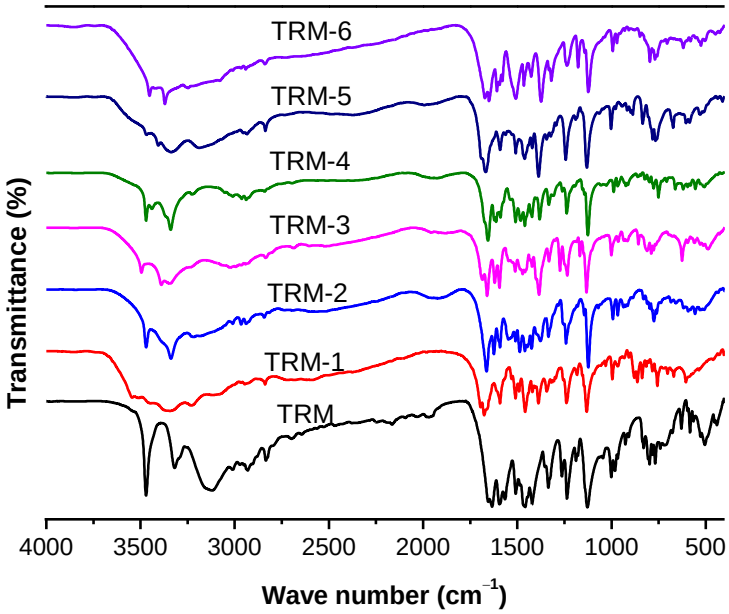

Figure 6.1 Comparison of vibrational spectroscopy of TRM and its molecular salts with isomeric HABA and ABA.

Differential Scanning Calorimetry (DSC). The melting temperatures of all the products are determined by DSC (Figure 6.2) and the values are compared with the starting components and found to be completely different from them suggesting the formation of pure products (Table 6.2). All products display water loss endothermic transitions near 100 °C except for TRM-4 which only exhibits single melting endotherm in the temperature range of 165–178 °C. The occurrence of a broad endothermic peak at < 100 °C for TRM-6 suggests the presence of water molecules in its crystal lattice. The broadness of the peak in the DSC plot for TRM-6 is because of the overlapping of the water loss endotherm with the melting endotherm.

Table 6.2 The comparison of melting onset endotherms of products with their respective starting materials.

API.	coformers	coformers Mt. Pt. (°C)	Product	water loss (°C)		salts Mt. Pt. (°C)	
				onset	peak	onset	peak
TRM [198–200 °C]	*o*-HBA	158	TRM-1	93	100	181	186
	m-HBA	202	TRM-2	130	137	166	176
	p-HBA	214	TRM-3	65	86	163	168
	o-ABA	146–148	TRM-4	-	-	165	168
	m-ABA	178–180	TRM-5	106	115	145	150
	p-ABA	287	TRM-6	-	-	70	90

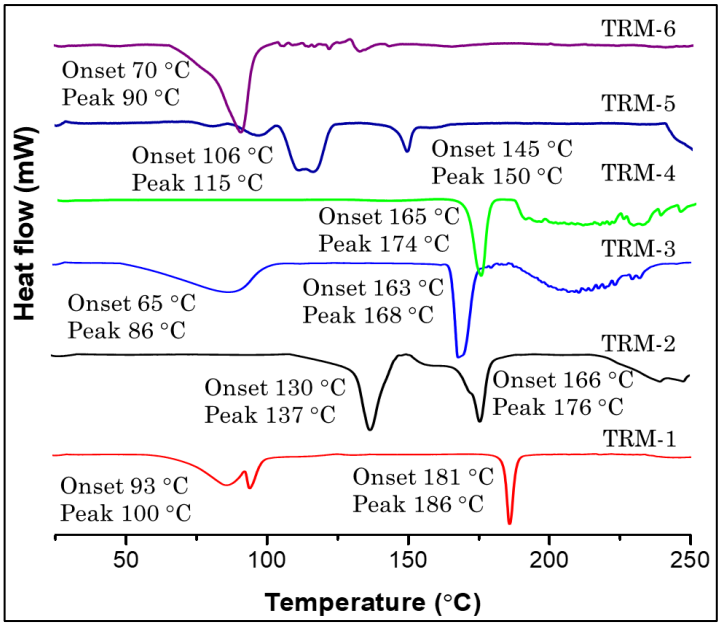

Figure 6.2 DSC endotherms represent the melting onset of TRM salts.

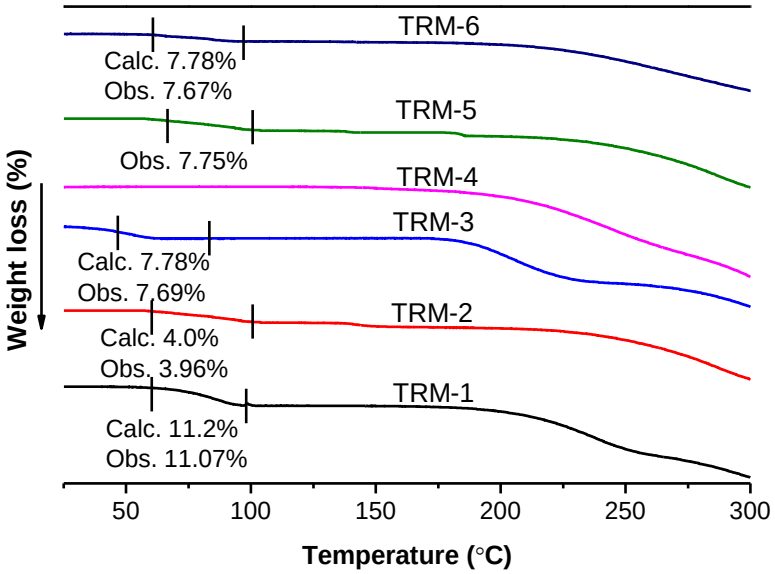

Figure 6.3 The weight loss estimated by TGA for hydrated products agrees well with the calculated values from the single crystal structures.

Thermogravimetric Analysis (TGA). The TGA plots and single crystal structural analysis are used to determine the water of crystallization content in the products and indicate the formation of hydrated structures for all products with different stoichiometry except for TRM-4 which is in anhydrous form (Figure 6.3). Weight loss of 11.07% is estimated for TRM-1 (calc 11.2%) by TG analysis below 100 °C suggesting trihydrate structure formation. The TG plot of TRM-2 shows 3.96% weight loss below 100 °C which indicates the release of one water molecule from its crystal lattice and matches with the monohydrate salt formation confirmed by single crystal X-ray analysis. The elimination of two water

molecules of crystallization from TRM-3 (obs 7.69% and calc 7.78%), TRM-5 (obs 7.75%), and TRM-6 (obs 7.67%) is estimated by TGA, and their presence in the crystal lattice of those salts are also confirmed by X-ray structural determination which will be discussed later.

Powder X-ray Diffraction (PXRD). The formation of molecular salts via mechanochemical grinding of API with two sets of isomeric coformers was also validated by PXRD analysis. The PXRD patterns of the products were compared with that of the TRM and their respective conformer and found to be distinct from them suggesting the formation of new solid phases (Figure 6.4). Besides Rietveld refinement was employed to check the phase purity of those products by comparing the experimental PXRD profile with the simulated from the single crystal structure (Appendix, Figure A9). The peak positions and patterns of PXRD for each product match with the simulated line, ensuring the formation of a single-phase solid.

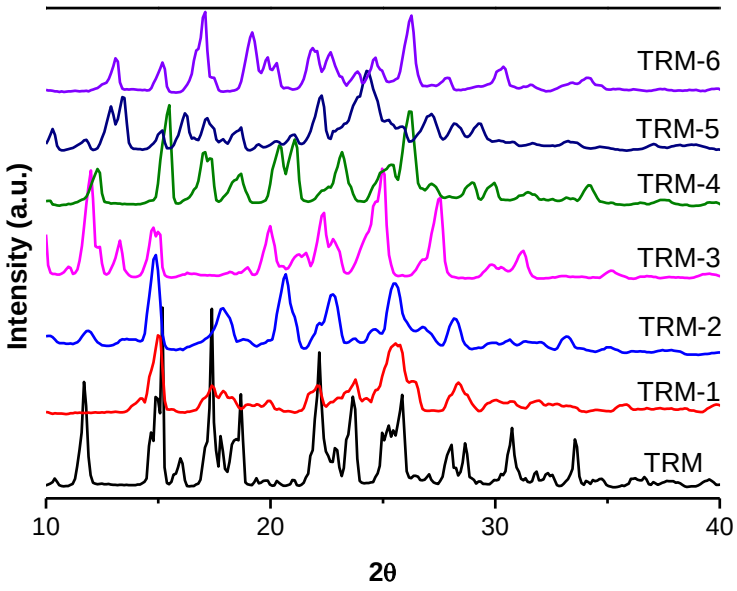

Figure 6.4 Overlaid PXRD patterns of TRM and its molecular salts.

Single Crystal X-RD. The crystal structures of five products were determined to examine the multicomponent structure-forming interactions between TRM and coformers. The crystal structural determination of TRM-5 was not successful because of the poor quality of the crystals. The formation of pure TRM-5 was confirmed by PXRD and DSC analysis. The formation of molecular salts was confirmed by the determination of proton location between the COOH group of coformers and the basic N center of the pyrimidine ring in the drug molecule. The proton distance parameters in the multicomponent solids are

available in Table 6.3 and indicate the formation of salt for the five products. Besides that the change in C–N–C bond angle and C–N bond length in the pyrimidine ring of the drug and O–C–O bond angle and C–O bond length parameters of carboxylic acid in the coformers show the formation of pyrimidine cation and carboxylate anion respectively (Table 6.3). The hydrogen bond parameters for the products are given in Table 6.4 and single crystal data are tabulated in Appendix Table A9.

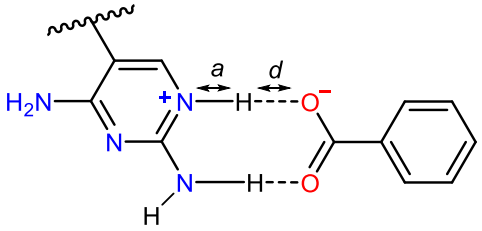

Figure 6.5 Pyrimidinium···carboxylate supramolecular interaction in the crystal structure of TRM salts.

Table 6.3 The acid proton distances from donor (*d*) and acceptor (a) atoms and bond angle and distance of basic N-atom of the pyrimidine ring and COOH group of the coformers in the salts (Figure 6.5).

product	distance (Å)		N–C (Å)	C–N–C angle (°)	C–O (Å)	O–C–O angle (°)	solid phase
	a	*d*					
TRM	-	-	1.34	115.5	1.32	121.21	-
TRM-1	0.88	1.75	1.36	117.8	1.28	121.46	salt
TRM-2	0.86	1.77	1.36	119.6	1.26	123.86	salt
TRM-3	0.88	1.80	1.36	119.9	1.27	123.14	salt
TRM-4	0.88	1.75	1.35	119.4	1.26	123.34	salt
TRM-6	0.86	1.82	1.35	119.5	1.26	122.62	salt

The crystal structure of TRM-1 was isolated as trihydrate from solution crystallization in the methanol and acetonitrile mixture. TRM-2 and TRM-3 crystallized as monohydrate and dihydrate from methanol and acetonitrile respectively. In the TRM-1 structure, protonated TRM and 2-hydroxybenzoate form $R_2^2(8)$ heterodimer via N^+–H···O^- and N–H···O hydrogen bonding. The heterodimers interact to form molecular tape through $R_2^2(8)$ ring motif homodimer of TRM molecules. The three water molecules of crystallization connect those molecular tapes to extend the structure of TRM-1 in 2D (Figure 6.6a). In TRM-2, the $R_2^2(8)$ ring motif drug-coformer heterodimers are connected by two parallel N–H···O hydrogen bonds formed between one of the NH_2 of the pyrimidine

ring of TRM and the oxygen atom of COO^- group of *m*-HBA (Figure 6.6b). The water dimer in the crystal lattice extends the layer structure of TRM-2 by forming hydrogen bonds with the OH and COO^- groups of *m*-HBA molecules. Similarly, water molecules serve as a linker between $R_2^2(8)$ ring motif heterodimers to form 1D molecular chains in the crystal structure of TRM-3 (Figure 6.6c). The structure is further extended in 2D by hydrogen bonding from one of the NH_2 groups of TRM to the oxygen atom of the middle ether group of another TRM molecule.

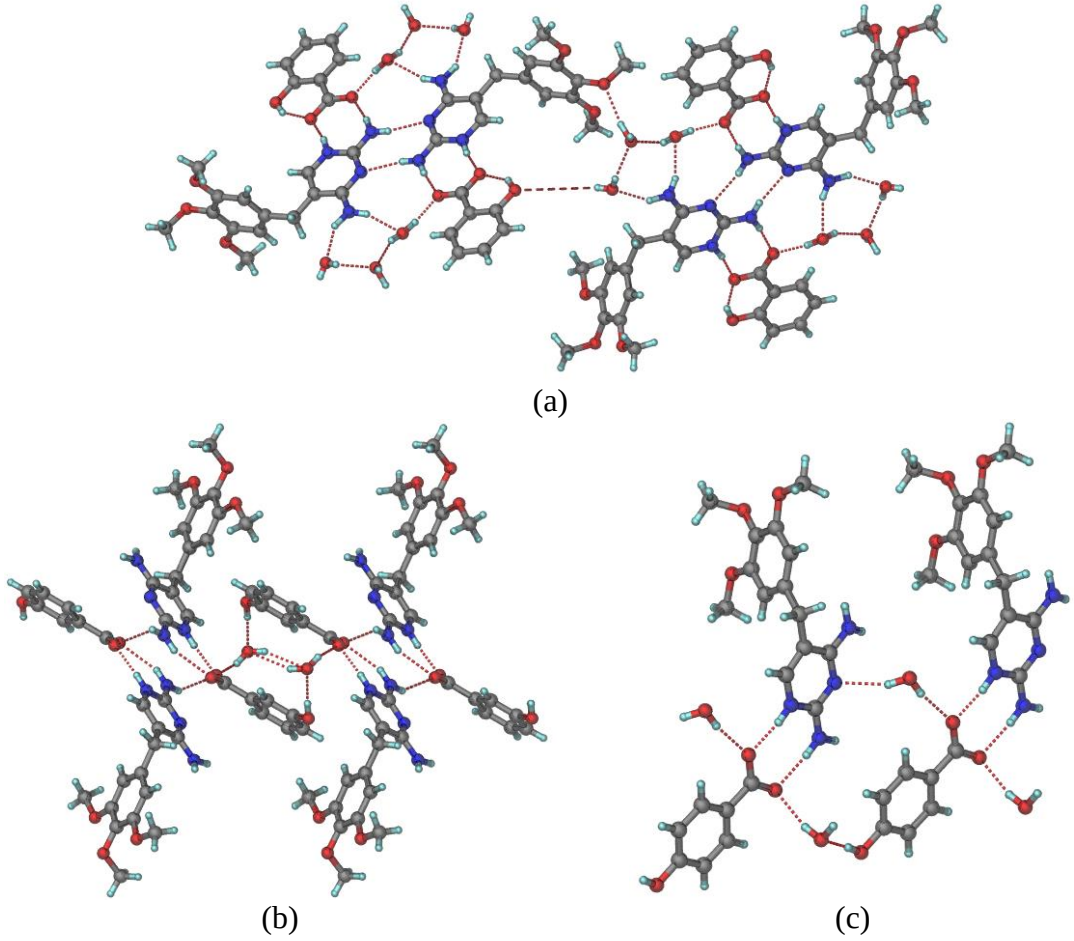

(a) (b) (c)

Figure 6.6 (a) Sheetlike structure of TRM-1 connected by water molecules via N–H···O and O–H···O interactions. (b) The layered structure of TRM-2 is connected by water molecules through O–H···O hydrogen bonds. (c) The drug-coformer dimers are linked by water molecules to form a 1D molecular chain in the crystal structure of TRM-3.

The crystal structures of the anhydrous salt of TRM with *o*-ABA display similar intermolecular interactions with TRM-2. The fundamental variation between the two structures is that the layered structure of TRM-2 is formed by hydrogen bonds between the water molecule and OH group of *m*-HBA, whereas in TRM-4 via hydrogen bonds between the NH_2 group of coformer and one of the oxygen atoms of COO^- group of the *o*-ABA.

The crystal structure of TRM-6 was obtained as dihydrate with a 1:1 ratio of drug TRM and *p*-ABA. The protonated N-center of the pyrimidine ring forms a one-point hydrogen-bonded synthon with one of the oxygen atoms of COO^- of the *p*-aminobenzoate while one of the amino group forms a two-point synthon with water molecule of crystallization. The *p*-aminobenzoates are further connected by water molecules via O–H···O interactions to form a 1D structure (Figure 6.7b). The structure further extends in 2D via hydrogen bonds from the NH_2 group of *p*-ABA to the oxygen atom of one of the ether moieties of TRM.

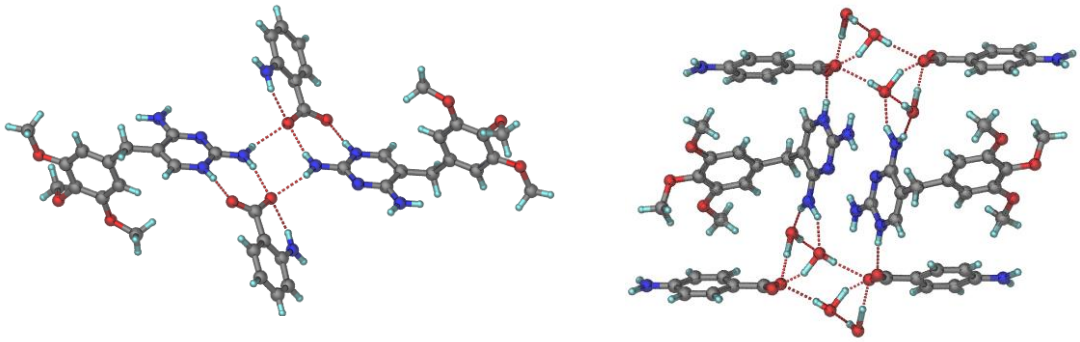

(a) (b)

Figure 6.7 (a) Pyrimidinium···carboxylate dimers in the crystal structure of TRM-4 are connected by N–H···O interactions. (b) The water molecules in the crystal structure of TRM-6 connect the drug and coformer molecules via N–H···O and O–H···O hydrogen bonds.

Table 6.4 Important hydrogen bond parameters observed in the molecular salts of TRM.

salts	interactions	H···A (Å)	D···A (Å)	∠D–H···A (°)	symmetry code
TRM-1	N_1–H_{1B}···O_5	1.90	2.740(8)	166	–1+x, y, z
	N_2–H_{2A}···N_3	2.24	3.095(7)	171	1–x, 1–y, 1–z
	N_2–H_{2B}···O_4	1.97	2.822(9)	170	–1+x, y, z
	O_6–H_6···O_5	1.77	2.504(7)	148	–
	O_7–H_{7A}···O_4	1.77	2.682(9)	166	–
TRM-2	N_1–H_{1B}···O_4	1.78	2.636(3)	176	1–x, 2–y, 1–z
	N_2–H_{2A}···O_5	2.17	2.924(4)	146	–1+x, y, 1+z
	N_2–H_{2B}···O_5	2.22	3.047(4)	160	1–x, 2–y, 1–z
	O_6–H_6···O_7	1.98	2.795(8)	177	1+x, y, z
	O_7–H_{7B}···O_4	1.98	2.695(6)	145	1–x, 2–y, 1–z
	O_7–H_{7A}···O_7	2.16	2.903(6)	153	1–x, 2–y, 1–z
TRM-3	N_1–H_{1B}···O_4	1.80	2.679(3)	172	–
	N_2–H_{2A}···O_5	1.94	2.820(3)	175	–
	N_2–H_{2B}···O_5	2.26	2.963(3)	137	2–x, –y, 1–z
	O_6–H_6···O_9	1.80	2.710(3)	177	x, 1+y, z
	O_8–H_{8A}···O_4	1.95	2.765(3)	170	–

	$O_8–H_{8B}\cdots N_3$	2.15	2.999(4)	160	x, 1+y, z
TRM-4	$N_1–H_{1B}\cdots O_4$	1.76	2.632(3)	174	–1+x, y, z
	$N_2–H_{2A}\cdots O_5$	2.11	2.898(3)	148	1–x, 1–y, 2–z
	$N_2–H_{2B}\cdots O_5$	1.94	2.794(3)	163	–1+x, y, z
	$N_5–H_{5C}\cdots O_5$	2.10	2.723(4)	127	–
TRM-6	$N_1–H_{1B}\cdots O_4$	1.83	2.652(5)	160	x, –1+y, z
	$N_2–H_{2B}\cdots N_3$	2.27	3.121(5)	172	1–x, –y, 1–z
	$N_4–H_{4A}\cdots O_6$	1.93	2.884(5)	155	1–x, 1–y, 1–z
	$N_4–H_{4B}\cdots O_7$	2.10	2.912(6)	166	1/2+x, 3/2–y, –1/2+z
	$O_7–H_{7B}\cdots O_6$	1.88	2.800(6)	175	3/2–x, –1/2+y, 3/2–z

6.3.3 Conformational variation of drug

The noncovalent interactions, molecular packing in the crystal lattice, and conformation of the molecules mainly determine the solubility and membrane permeation properties of drug molecules. The intermolecular interactions and molecular packing of the TRM are changed due to salt formation with the two sets of coformers. Although the drug has a flexible methylene group that links the phenyl and pyrimidine rings, the conformation of TRM is significantly changed only in product TRM-1 (Figure 6.8).

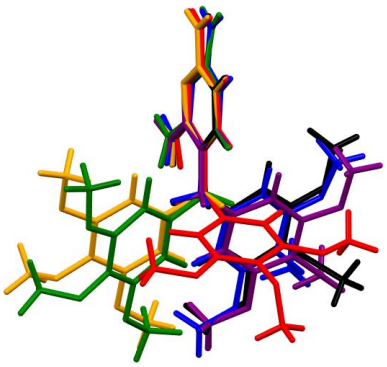

Figure 6.8 An overlay of molecular conformers of TRM extracted from its molecular salt crystal structures. [TRM (green), TRM-1 (red), TRM-2 (blue), TRM-3 (black), TRM-4 (orange), and TRM-6 (purple)].

The torsion angle of the methylene group in the crystal structure of pure TRM is 89°. The angle increases to 177° in the structure of TRM-1 while it slightly decreases for the remaining products, i.e., in the range of 70–80° (Figure 6.9). Such variation in the torsion angle causes the difference in the orientation of the functional group of TRM could influence the solute···solvent interaction and has an impact on the solubility and membrane permeation.

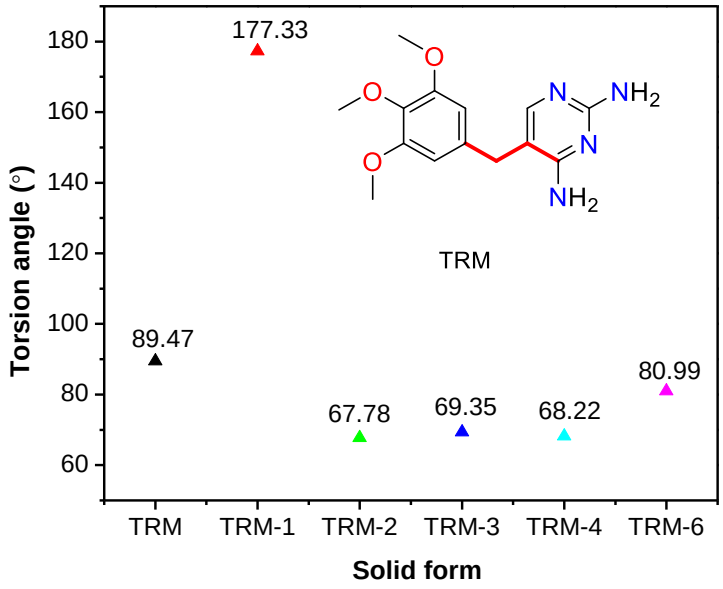

Figure 6.9 Torsion angle of flexible methylene group in pure TRM and its molecular salts.

6.3.4 Solubility Measurement

The solubility of powder samples of the TRM-1 to TRM-6 was evaluated at room temperature in three different pH media and compared with the pure TRM (Figure 6.10). At pH 1.2, only salts of *para*-substituted coformers display improved solubility than the parent TRM, while the remaining products exhibit comparable solubility. The PXRD analysis of the undissolved samples (residuals) retrieved from the 1.2 pH buffer at 12 h shows that the salt products are transformed into trimethoprim hydrochloride except for TRM-1 in which its PXRD patterns remain unchanged (Appendix Figure A10a, b). The formation of chloride salt for the molecular salts at pH 1.2 is the reason for their observed comparable solubility with pure TRM as it also forms chloride salt at low pH conditions. In aqueous and pH 7.4 media, both sets of coformers afford molecular salts with improved solubility in the order of *meta*-substituted coformers followed by *para*-substituted and *ortho*-substituted, except for the salt of *para*-ABA (TRM-6) that displays higher solubility than salt of *meta*-ABA (TRM-5) at pH 7.4. At both media, salts of isomeric ABA demonstrate better solubility than salts of isomeric HBA. One of the hydrogen atoms of the NH_2 group of the ABA is free and available for solute···solvent interaction with the water molecule leads to higher solubility, whereas the OH group of HBA is not free because it is involved in hydrogen bonding in the salts. The phase stability study of the products was performed at pH 7.4 and presented in Appendix A10c. All the multicomponent crystals are found to be stable, except for TRM-5 which dissociates into starting materials.

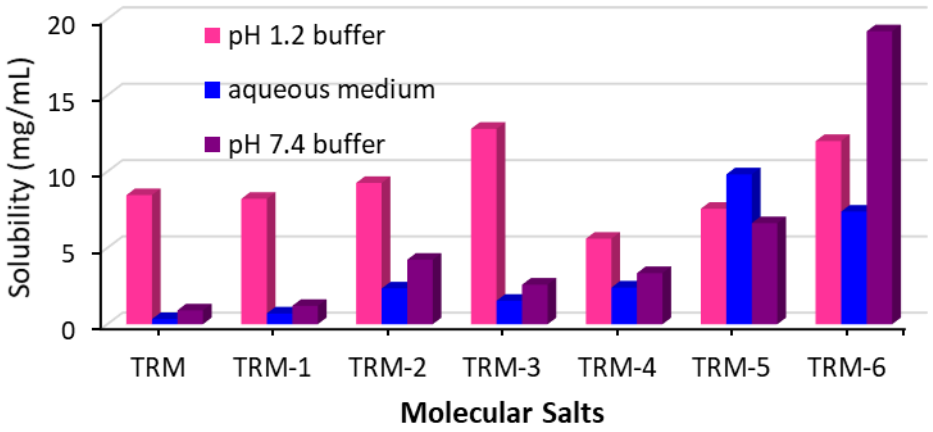

Figure 6.10 Solubility of trimethoprim comparison with its molecular salts in three different pH conditions.

To comprehend the difference observed in the solubility parameter, the molecular packing energy of the materials was calculated using Mercury 4.2 coupled with CSDS 2023. The higher the negative packing energy value of solid material, the higher will be its thermodynamic stability. Consequently, it shows lower thermodynamic properties. The obtained packing energy values show that the stability order for the salts of HBA: TRM-2 (E = −17 kJ mol^{-1}) < TRM-3 (E = −86 kJ mol^{-1}) < TRM-1 (E = −116 kJ mol^{-1}), supporting the observed solubility trend in aqueous and pH 7.4 buffer media, i.e., TRM-2 > TRM-3 > TRM-1.

The strength of structure forming interactions between various functional groups of the drug and coformers also determine the thermodynamic properties of the multicomponent crystals. Strong ionic supramolecular synthon 1 is formed as a main hydrogen bonding interaction between pyrimidine moiety and acid group in the crystal structures of TRM-1 to TRM-4, whereas in the TRM-6 the interaction between the pyrimidine ring of TRM and acid group of *para*-ABA form weaker one-point synthon 2 (Figure 6.11). The energy value for the interactions was computed on Gaussian 09 with the level of theory B3LYP/6-311G*(d,p) (Figure 6.12). The formation of weaker intermolecular interactions suggests higher solubility. The strength of the synthon 1 in the salts of HBA follows in the order of TRM-2 (E = −17.2 kcal mol^{-1}) < TRM-3 (E = −20.7 kcal mol^{-1}) < TRM-1 (E = −25.4 kcal mol^{-1}) which can be one of the reasons for the solubility trend displayed by the salts in pure water and at pH 7.4. Similarly in the salts of ABA, the formation of weaker synthon 2 in TRM-6 (E = 0 kcal mol^{-1}) as compared to synthon 1 of TRM-4 (E = −14.8 kcal mol^{-1}) making the solubility of TRM-6 is higher.

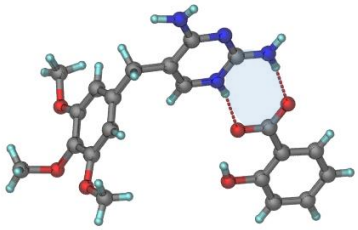

Synthon 1
TRM-1 to TRM-4
(a)

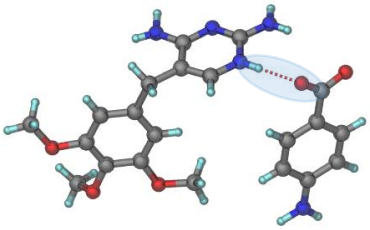

Synthon 2
TRM-6
(b)

Figure 6.11 The prime hydrogen bonding interactions of TRM with isomeric HBA and ABA in the crystal structures of (a) TRM-1 to TRM-4 and (b) TRM-6.

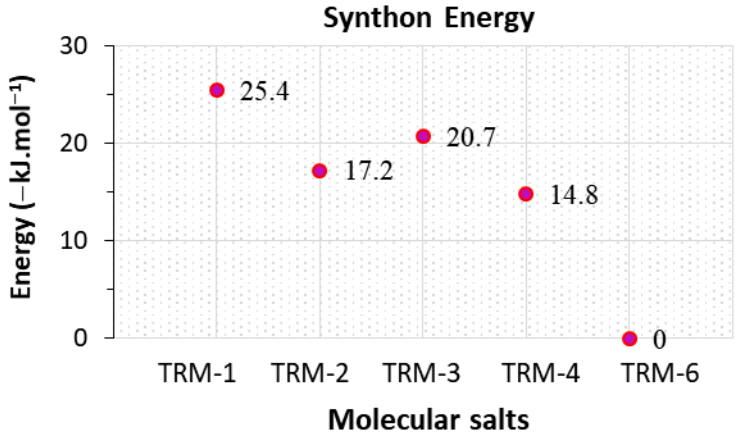

Figure 6.12 Relative energy values of the prime hydrogen-bonded synthon in the crystal structures of salts of TRM.

6.3.5 Membrane Permeation Behaviour

The permeation property of the multicomponent crystals TRM-1 to TRM-6 was measured and compared with the pure TRM at pH 7.4 and 1.2 (Figures 6.13 and 6.14). The multi-component crystalline phases display a higher release rate and drug flux than the pure TRM. At pH 1.2, both release rate and amount of drug flux are highest for salts of *para*-substituted coformers (TRM-3 and TRM-6). The reason for such high permeation is due to their high solubility results in a higher concentration density over the membrane making the movement drug faster. The rate of permeation for TRM-1 is slower than pure TRM at the beginning and showed a sharp increase after 20 min.

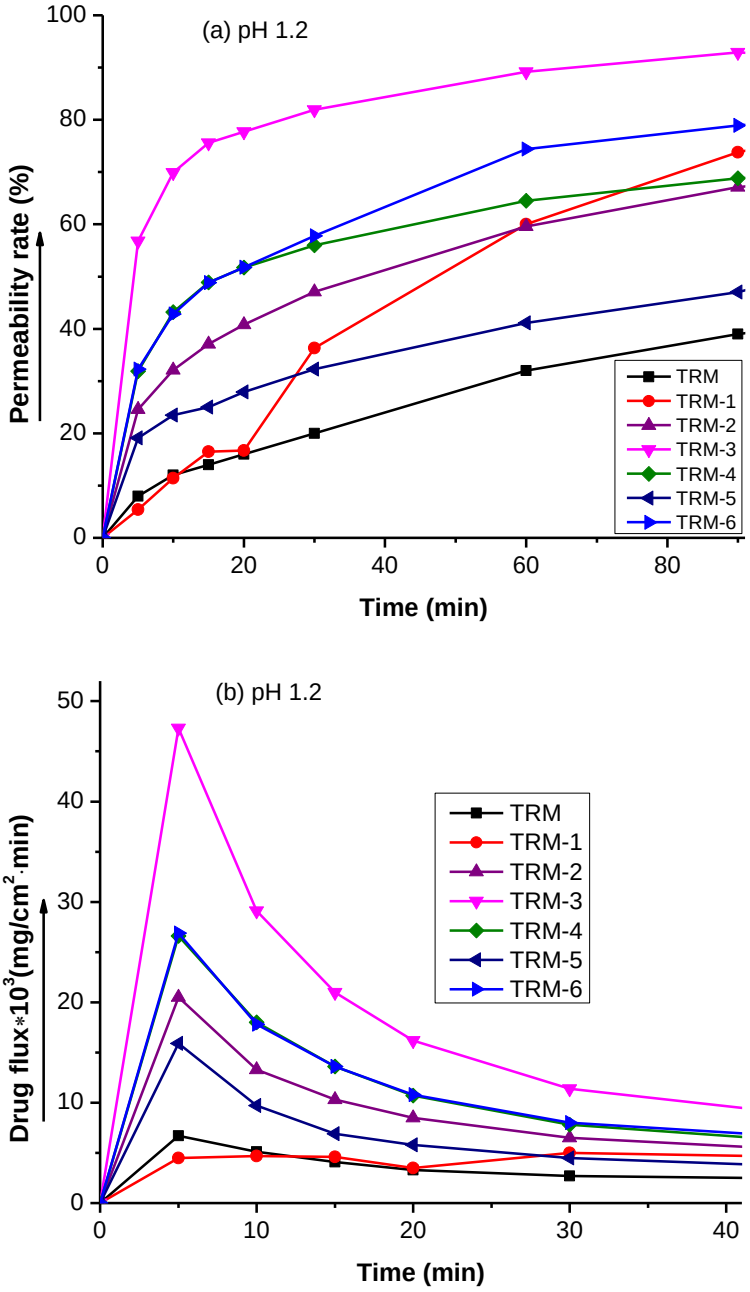

Figure 6.13. (a) Permeation rate and (b) drug flux of molecular salts of TRM with isomeric HBA and ABA at pH 1.2.

The molecular salts demonstrate a higher permeation rate and drug flux than the parent drug at pH 7.4 (Figure 6.14). TRM-2, TRM-3, and TRM-6 show high and similar permeation rates among the products. The reason for such similarity can be the similarity of the drug conformation in their crystal structures (Figure 6.8). The increase in the drug flux of the products in the order of *meta*-substituted (TRM-2 and TRM-5) > *para*-substituted (TRM-3 and TRM-6) > *ortho*-substituted (TRM-1 and TRM-4) > TRM is attributed to their solubility values [solubility values in mg/mL at pH 7.4: TRM-6 (19.19), TRM-5 (6.62), TRM-2 (4.23), TRM-4 (3.35), TRM-3 (2.59), TRM-1 (1.20), and TRM

(0.91)]. The higher the solubility of the drug, the density will be its concentration across the membrane and the amount of drug flux.

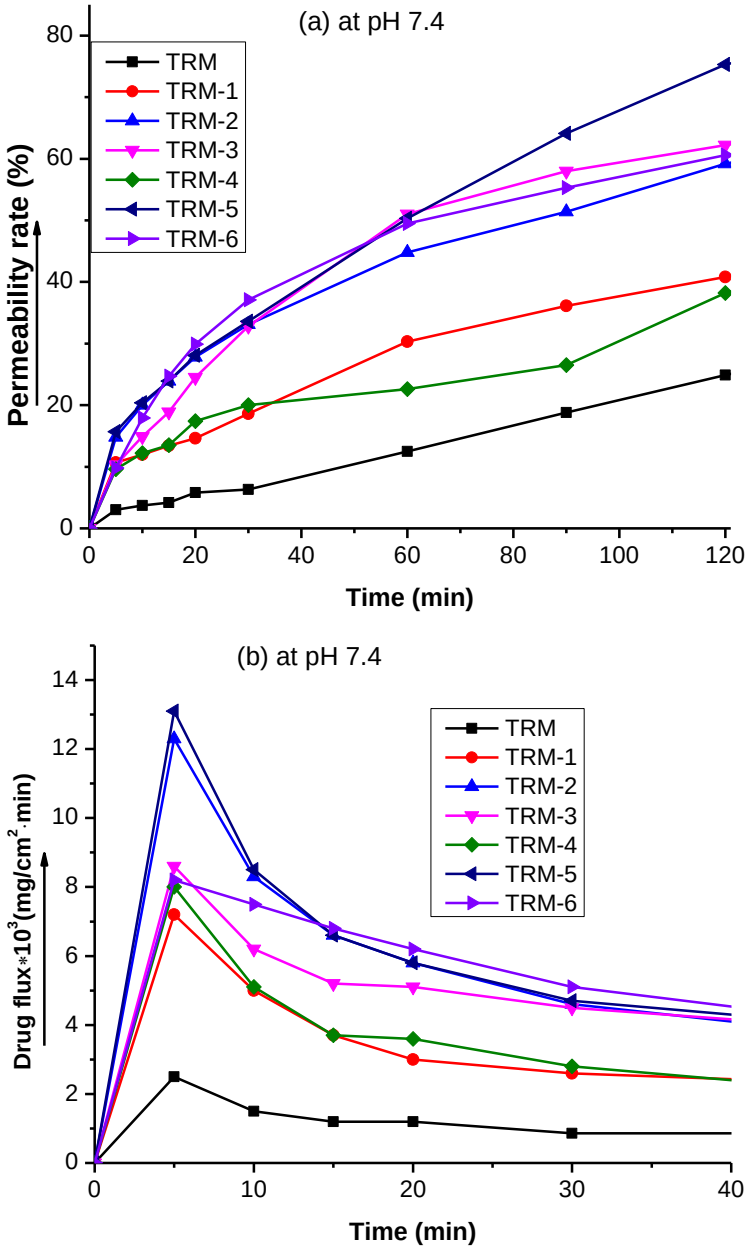

Figure 6.14. (a) Permeation rate and (b) drug flux of molecular salts of TRM with isomeric HBA and ABA at pH 7.4.

6.3.6 Hirshfeld Surface Analysis

Hirshfeld analysis was carried out to understand the role of noncovalent interactions on the solubility and membrane permeation parameters of the multicomponent crystals. Figure 6.15 demonstrates the contribution of various interactions in each molecular salt and parent API. The polar O–H interaction percentage in TRM-4 (20.9%) and TRM-3 (22.6) are lower than that of the TRM-6 (28%), TRM-1 (28.5%), and TRM-2 (28.8) which

makes TRM-4 and TRM-3 less polar. Hence, compounds with less polarity display a higher partition coefficient in polar media, i.e., higher lipophilicity and eventually higher permeation rate. Though the solubility of TRM-4 is the lowest among all products at pH 1.2, it demonstrates a higher permeation rate and drug flux because of its higher lipophilicity. At pH 7.4, the observed release rate of the products is generally found to be against their lipophilic nature. The O–H interaction contribution in TRM-2 and TRM-6 is relatively higher and makes them less lipophilic as compared to the others. However, they display higher permeation because of high solubility at pH 7.4 which results in a higher concentration in the absorption site and makes the diffusion faster through the membrane.

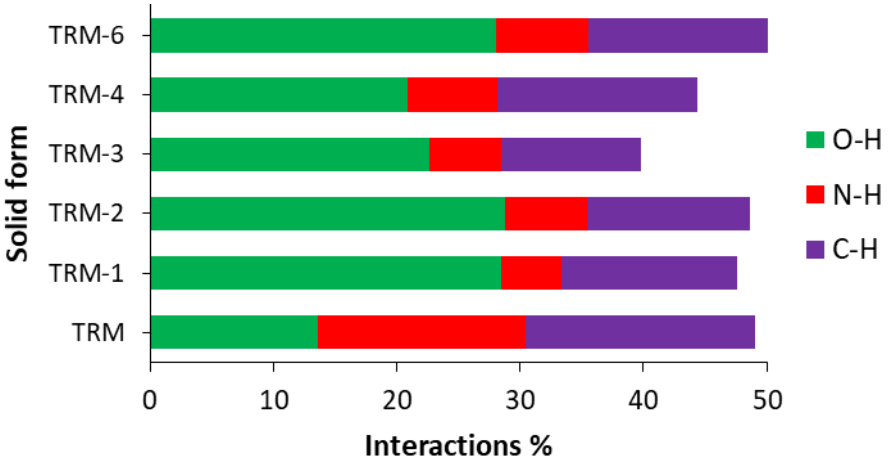

Figure 6.15 Various noncovalent interactions percentage present in the TRM and its molecular salts.

6.4 Summary

Six molecular salts of the low bioavailable drug TRM were synthesized via liquid-assisted grinding with isomeric hydroxybenzoic acids and isomeric aminobenzoic acids. Molecular salts demonstrated higher solubility and membrane permeability than the parent API. The role of variation in the functional groups and their isomeric positions in modulating the physicochemical property of the drug was investigated. The improved properties exhibited by these solid forms are attributed to a conformation change in the drug molecule, variation in the strength of intermolecular interactions and molecular packing in the crystal lattice, and solute···solvent interactions.

6.5 Experimental Section

6.5.1 Materials

Drug TRM (purity ~99%) and coformers were purchased from Yarrow chem products and Sigma-Aldrich, India respectively. HPLC-grade methanol, ethanol, and acetonitrile were purchased from SRL, India, and used without further purification. Buffer solutions for the solubility and permeability studies were prepared using Millipore water.

6.5.2 Synthesis of Molecular Salts

The product materials were synthesized by grinding a 1:1 ratio of TRM and coformers by adding 3-5 drops of ethanol for about 1 hr. The powder sample was dissolved in methanol, acetonitrile, or a mixture of both solvents and kept at room temperature to obtain single crystals. Good quality crystals grew after a few days for TRM-1 to TRM-4 and TRM-6 and were analyzed by single crystal XRD, PXRD, DSC, TGA, and FT-IR. We couldn't get suitable crystals for TRM-5. Hence, the ground powder sample was used to evaluate the formation of product TRM-5.

6.5.3 Vibrational Spectroscopy

PerkinElmer Frontier FTIR spectrophotometer was used to record the IR spectra of the product materials in the range of 400–4000 cm^{-1} (Figure 5.1). The major functional groups stretching frequencies (cm^{-1}) for TRM and its products are listed as follows, TRM: 3470–3320 (N–H), 3125 (aromatic C–H), 1660 (C=N), 1596 (C=C), 1335(C–N), 1236 and 1128 (C–O); TRM-1: 3540 (OH), 3342–3225 (N−H), 3102 (aromatic C−H), 1676 (C=N), 1592 (C=C), 1388 (COO^-), 1343 (C–N), 1239 & 1132 (C–O); TRM-2: 3470 (OH), 3338–3214 (N–H), 3008 (aromatic C−H), 1663 (C=N), 1622 (C=C), 1378 (COO^-), 1335 (C–N), 1242 and 1123 (C–O); TRM-3: 3495 (O–H), 3388–3343 (N–H), 3025 (aromatic C−H), 1661 (C=N), 1612 (C=C), 1384 (COO^-), 1332 (C–N), 1235 and 1133 (C–O); TRM-4: 3470–3339 (N–H), 3049 (aromatic C−H), 1655 (C=N), 1611 (C=C), 1381 (COO^-), 1333(C–N), 1238 and 1125 (C–O); TRM-5: 3337–3188 (N–H), 1697 (C=N), 1591 (C=C), 1388 (COO^-), 1243 and 1131 (C–O); TRM-6: 3453–3371 (N–H), 3079 (aromatic C−H), 1649 (C=N), 1593 (C=C), 1374 (COO^-), 1319 (C−N), 1236 and 1123 (C–O).

6.5.4 Differential Scanning Calorimetry (DSC)

The DSC thermograms of the product samples were recorded on Mettler Toledo DSC 822e. 5 mg of the sample was taken in a pan and closed with aluminum foil. The pan with the sample was heated in the range of 25−250 °C under dry nitrogen at constant flow at a 30 mL/min rate. The instrument was calibrated by melting pure indium before recording the samples.

6.5.5 Thermogravimetric Analysis (TGA)

The TGA data were recorded on the Mettler Toledo TGA/SDTA 851e module. 4−6 mg of the material was taken in the pan and sealed. The pan with the sample was heated at a temperature range of 25−300 °C with a 10 °C/min rate under dry nitrogen that flow at 30 mL/min rate.

6.5.6 Powder X-ray Diffraction (PXRD)

The PXRD patterns of the samples were analyzed on a Bruker D8 Focus X-ray diffractometer, Germany using Cu-Kα X-radiation (λ = 1.54056 Å) at 35 kV and 25 mA. The data collection was performed in a 10–40° 2θ range at a 1° min^{-1} scan rate.

6.5.7 Single Crystal X-ray Diffraction (Single Crystal X-RD)

The single crystal data collection was carried out on a Bruker APEX-II CCD diffractometer with radiation of Mo Kα (λ = 0.71073 Å). Bruker SAINT Software was used to reduce data reduction. SADABS was used to correct the intensity of absorption. SHELXL software was used to solve and refine the single crystal structures of the products. The key crystallographic data of the molecular salts are tabulated in Appendix Table A9. Hydrogen bond parameters are listed in Table 6.4.

6.5.8 Hirshfeld Surface Analysis

The contribution percentage of various intermolecular interactions of the salt products was calculated using Crystal Explorer version 21 at the B3LYP/6-31G *(d, p) level of theory (Figures 6.15).

6.5.9 DFT Calculation

The energy values of the hydrogen-bonded synthons in the crystal structure of the molecular salt were computed using Gaussian09 on DFT with B3LYP; 6311G *(d, p) as the basic level (Figure 6.12).

6.5.10 Cambridge Structural Database (CSD)

The CSD survey was carried out with the latest version, CSD 2023.1 software coupled with Mercury 4.2.0. An overlay of drug conformers extracted from the crystal structures of the molecular salts was drawn on Mercury4.2 linked to Cambridge Structural Data (Figure 6.8).

6.5.11 Solubility Measurements

An unknown quantity of the sample was dissolved in 2.5 mL of aqueous medium, buffer solution of pH 1.2 and 7.4. The prepared samples were continuously stirred at a rate of 700 rpm for 12 h. The sample solution was filtered and the absorbance of the filtrates was recorded on UV–visible double-beam spectrophotometer. The amount of products dissolved in the three different media (C_u) was obtained from the calibration curves with the formula $C_u = (A_u - \text{intercept})/\text{slope}$, where A_u is the absorbance of the filtered solution. The solubility values are the average measurements of two experiments.

6.5.12 Membrane Permeability

The permeability experiment was carried out using a dialysis membrane. A 5 mg of sample was prepared in the membrane as a donor chamber and placed in the diffusion apparatus that contains 100 mL 1.2 or 7.4 pH buffer solution. The solution in the diffusion apparatus was continuously stirred at a rate of 700 rpm at 26 °C and the sample permits through the membrane to the solution. 3 mL of the sample was pipetted from the solution in a specific time interval. An equivalent amount of fresh solution was introduced into the diffusion apparatus to keep the amount of the solution constant. UV–vis spectrophotometry was used to analyze the quantity of the material permitted via the membrane at definite time intervals.

6.6 References

[1] Amidon, G. L., Lennernäs, H., Shah, V. P., and Crison, J. R. A theoretical basis for a biopharmaceutic drug classification: the correlation of in vitro drug product dissolution and in vivo bioavailability. *Pharmaceutical research*, 12(3):413-420, 1995.

[2] Qiu, Y., Chen, Y., Zhang, G. G. Z., Yu, L., and Mantri, R. V. *Developing Solid Oral Dosage Forms: Pharmaceutical Theory and Practice*. Academic Press; 2016.

[3] Arnott, J. A. and Planey, S. L. The influence of lipophilicity in drug discovery and

design. *Expert opinion on drug discovery*, 7(10):863-875, 2012.

[4] Testa, B., Crivori, P., Reist, M., and Carrupt, P.-A. The influence of lipophilicity on the pharmacokinetic behavior of drugs: Concepts and examples. *Perspectives in Drug Discovery and Design*, 19:179-211, 2000.

[5] Naylor, M. R., Ly, A. M., Handford, M. J., Ramos, D. P., Pye, C. R., Furukawa, A., Klein, V. G., Noland, R. P., Edmondson, Q., Turmon, A. C., Hewitt, W. M., Schwochert, J., Townsend, C. E., Kelly, C. N., Blanco, M.-J., and Lokey, R. S. Lipophilic Permeability Efficiency Reconciles the Opposing Roles of Lipophilicity in Membrane Permeability and Aqueous Solubility. *Journal of Medicinal Chemistry*, 61(24):11169-11182, 2018.

[6] Zeleke, T. Y. and Sarma, B. Isomeric Coformer Responsive Conformational Adjustment to Recuperate Stability, Solubility, and In Vitro Permeation Behavior of Drug Molecular Salts. *Crystal Growth & Design*, 22(12):7405–7418, 2022.

[7] Haskins, M. M., Kavanagh, O. N., Sanii, R., Khorasani, S., Chen, J.-M., Zhang, Z.-Y., Dai, X.-L., Ren, B.-Y., Lu, T.-B., and Zaworotko, M. J. Tuning the Pharmacokinetic Performance of Quercetin by Cocrystallization. *Crystal Growth & Design*, June 20232023.

[8] Meng, S.-S., Yu, Y.-M., Bu, F.-Z., Yan, C.-W., Wu, Z.-Y., and Li, Y.-T. Directional Self-Assembly of Ofloxacin and Syringic Acid: The First Salt Cocrystal of Ofloxacin with Phenolic Acid Displays Superior In Vitro/Vivo Biopharmaceutical Property and Enhanced Antibacterial Activity. *Crystal Growth & Design*, 22(11):6735-6750, 2022.

[9] Mannava, M. K. C., Garai, A., and Nangia, A. K. Diffusion and Flux Improvement of Drugs through Complexation. *Molecular Pharmaceutics*, 20(5):2293-2316, 2023.

[10] Allu, S., Garai, A., Chernyshev, V. V, and Nangia, A. K. Synthesis of Ternary Cocrystals, Salts, and Hydrates of Acefylline with Enhanced Dissolution and High Permeability. *Crystal Growth & Design*, 22(7):4165-4181, 2022.

[11] Sanphui, P., Devi, V. K., Clara, D., Malviya, N., Ganguly, S., and Desiraju, G. R. Cocrystals of Hydrochlorothiazide: Solubility and Diffusion/Permeability Enhancements through Drug–Coformer Interactions. *Molecular Pharmaceutics*, 12(5):1615-1622, 2015.

[12] Segalina, A., Pavan, B., Ferretti, V., Spizzo, F., Botti, G., Bianchi, A., Pastore, M., and Dalpiaz, A. Cocrystals of Nitrofurantoin: How Coformers Can Modify Its

Solubility and Permeability Across Intestinal Cell Monolayers. *Crystal Growth & Design*, 22(5):3090-3106, 2022.

[13] Ji, X., Wu, D., Li, C., Li, J., Sun, Q., Chang, D., Yin, Q., Zhou, L., Xie, C., Gong, J., and Chen, W. Enhanced Solubility, Dissolution, and Permeability of Abacavir by Salt and Cocrystal Formation. *Crystal Growth & Design*, 22(1):428-440, 2022.

[14] Shajan, D. K., Pandey, N., Ghosh, A., Chanduluru, H. K., and Sanphui, P. Investigating the Effect of Emtricitabine Cocrystals with Aromatic Carboxylic Acids on Solubility and Diffusion Permeability. *Crystal Growth & Design*, 23(7):5289-5300, 2023.

[15] Budziak-Wieczorek, I., and Maciołek, U. Synthesis and Characterization of a (−)-Epicatechin and Barbituric Acid Cocrystal: Single-Crystal X-ray Diffraction and Vibrational Spectroscopic Studies. *ACS Omega*, 6(12):8199-8209, 2021.

[16] Gunnam, A. and Nangia, A. K. Novel Hydrate and Anhydrate Cocrystals/Salts of Norfloxacin and Their Physicochemical Properties. *Crystal Growth & Design*, May 20232023.

[17] Schultheiss, N. and Newman, A. Pharmaceutical Cocrystals and Their Physicochemical Properties. *Crystal Growth & Design*, 9(6):2950-2967, 2009.

[18] Ren, B.-Y., Dai, X.-L., Zhang, F., Long, X., Huang, Y.-L., Chen, J.-M., and Lu, T.-B. "Drug–Coformer–Drug" Multicomponent Crystals to Simultaneously Improve the Solubility of Two Insoluble Combined Drugs by Introduction of a Soluble Coformer. *Crystal Growth & Design*, 22(10):5785-5790, 2022.

[19] Khatioda, R., Saikia, B., Das, P. J., and Sarma, B. Solubility and in vitro drug permeation behavior of ethenzamide cocrystals regulated in physiological pH environments. *CrystEngComm*, 19(46):6992-7000, 2017.

[20] Saikia, B., Sultana, N., Kaushik, T., and Sarma, B. Engineering a Remedy to Improve Phase Stability of Famotidine under Physiological pH Environments. *Crystal Growth and Design*, 19(11):6472-6481, 2019.

[21] Yuliandra, Y., Hutabarat, L. J., Ardila, R., Octavia, M. D., and Zaini, E. Enhancing solubility and antibacterial activity using multicomponent crystals of trimethoprim and malic acid. *Pharm Educ*, 21(2):296-304, 2021.

[22] Bhattacharya, B., Das, S., Lal, G., Soni, S. R., Ghosh, A., Reddy, C. M., and Ghosh, S. Screening, crystal structures and solubility studies of a series of multidrug salt hydrates and cocrystals of fenamic acids with trimethoprim and sulfamethazine. *Journal of Molecular Structure*, 1199:127028, 2020.

[23] Zheng, Q., Unruh, D. K., and Hutchins, K. M. Cocrystallization of trimethoprim and solubility enhancement via salt formation. *Crystal Growth & Design*, 21(3):1507-1517, 2021.

[24] Maity, D. K., Paul, R. K., and Desiraju, G. R. Drug–drug binary solids of nitrofurantoin and trimethoprim: crystal engineering and pharmaceutical properties. *Molecular Pharmaceutics*, 17(12):4435-4442, 2020.

[25] Ma, L., Zheng, Q., Unruh, D. K., and Hutchins, K. M. Reversible interconversion of pharmaceutical salt polymorphs facilitated by mechanical methods. *Chemical Communications*, 59(50):7779-7782, 2023.

[26] Muthiah, P. T., Francis, S., Rychlewska, U., and Warżajtis, B. Crystal engineering of analogous and homologous organic compounds: hydrogen bonding patterns in trimethoprim hydrogen phthalate and trimethoprim hydrogen adipate. *Beilstein Journal of Organic Chemistry*, 2(1):8, 2006.

[27] Umadevi, B., Prabakaran, P., and Muthiah, P. T. A pseudo-quadruple hydrogen-bonding motif consisting of six N—H··· O hydrogen bonds in trimethoprim formate. *Acta Crystallographica Section C: Crystal Structure Communications*, 58(8):o510-o512, 2002.

[28] Subashini, A., Muthiah, P. T., Bocelli, G., and Cantoni, A. Hydrogen Bonding Patterns in Trimethoprimium Cinnamate 1.52 Hydrate. *Journal of Chemical Crystallography*, 41(7):976-979, 2011.